Study on the hydrodynamic characteristics of swirl flow device

Dildora Badalova[1*], *Abdumalik* Badalov[1]

[1]Tashkent State Technical University, 100095 Tashkent, Uzbekistan

Abstract. The work examined the hydrodynamic situation, which is created by the interaction of reciprocal twisted flows and the distribution of axial velocity along the radius of the primary and secondary flow inputs and the radius of the exhaust pipe in order to create a complete physical picture. Determination of the radius distribution of the static pressure values determined by the height of the apparatus and the static pressure distribution in the exhaust pipe.

1. Introduction

At present, great attention is paid to the environmental safety of industrial plants, including the cleaning of air emissions of enterprises from dust. Industrial enterprises emit millions of tons of dust from combustion of fossil fuels, cement production, metallurgical industry etc. industries into the atmosphere per year [1, 2, 3]. One of the promising types of equipment for cleaning dust emissions are inertial dust collectors, which are used in the primary stages of air purification from dust, which allows to significantly reduce air pollution, as well as to reduce the load on subsequent gas cleaning devices and reduce their wear. Inertial dust collectors are classified as dry mechanical dust collectors [4]. In inertial systems, the flow of dust particles suspended in the gas stream undergoes a sharp change in the direction of movement, with the dust particles not moving behind the stream due to high inertia, causing inertial forces that seek to eject particles from the stream. As a result, the dust particles are pressed against the walls of the dust collector and then dropped into the silo. The advantages of inertial dust collectors are small dimensions and low metal capacity due to the relatively high rate of input of dust gas (15-25 m/s) into cleaning devices [4]. Among the inertial dust collectors, the most common are jet-inertial dust collectors with counter-twisted streams, which have high dust-cleaning efficiency and low dust flow resistance.

Simulation of dust traps with counter-twisted streams requires a comprehensive study of the hydrodynamic situation that is created by interaction of counter-twisted streams. The work investigated the axial velocity distribution by the radius of the primary and secondary flow inputs and by the radius of the exhaust pipe in order to provide a complete physical picture, because very little research has been done for spun-back collectors [5]. A large number of works is devoted to the distribution of fields of velocities on the cross section of the apparatus [5, 6, 7, 8].

All measurements of the axial velocity were carried out in the gas phase, since in [6] it was shown that the velocity fields of air flows are practically not deformed at the introduction of solid phase.

The distinguishing feature of the twisted flows (in particular the counter twisted flows) is the presence of a radial gradient of static pressure associated with the presence of a tangential component of the gas velocity. The work determined the distribution of the static pressure values determined by the height of the apparatus and the static pressure distribution in the exhaust pipe. All the above-mentioned hydrodynamic characteristics have a significant impact on the main technical and economic characteristics of the counterflow dust catcher (efficiency of capture and loss of pressure).

2. Methods

The axial velocity distribution over the radius of the primary and secondary inputs and the radius of the exhaust pipe and the static pressure distribution were determined by a five-channel ball probe with a sensitive element diameter of 9 mm [7].

In measurements, the angle σ was determined by the coefficient:

*Corresponding author: abdumalikovna1987@gmail.com

$$K_\sigma = \frac{h_3 - h_1}{h_2 - h_4} = \frac{K_3 - K_1}{K_2 - K_4} \quad (1)$$

The value of K_σ was determined by the equation (1) and the calibration graph contained the angle σ [7], which determined the value of coefficients

$$K_2 \; ; (K_2 - K_4) \; ; (K_3 - K_1) \; .$$

The calculation of static pressure and velocity at any point was based on the following equations:

$$h_{ст} - h_a = \frac{K_m * m}{1 + 0.001(t-15)} * \frac{760(273+t)}{B*273} * \frac{\rho_ж * \gamma_r}{\rho_b * 1000} * \left(h_2 - K_2 * \frac{h_2 - h_4}{K_2 - K_4}\right) \quad (2)$$

$$V = \sqrt{K_m} * \sqrt{m} * \frac{1}{\sqrt{1+0.001(t-15)}} * \sqrt{\frac{760(273+t)}{B*273}} ** \sqrt{\frac{\gamma_r}{\rho_r} * \left(\frac{h_3 - h_1}{K_3 - K_1} - \frac{h_2 - h_4}{K_2 - K_4}\right)} * \sqrt{\frac{\rho_ж}{\rho_b * 1000}} \quad (3)$$

where $K_m = K_1 * K_2 * K_3 * K_4$ – micromanometer ratio;

The component V_z was determined by dependence:

$$V_z = -V * \cos\sigma * \sin\varphi \quad (4)$$

Equations (1), (2), (3) were computed using computers.

The probe was calibrated by a Prandtl reference tube in a wind tunnel with a strict flow orientation in space [7]. The Prandtl tube determined $h_{ст}$ и $h_{ск}$.

3. Results

As noted above (paragraph.1.2.), a characteristic feature of twisted flows is the significant gradient of static pressure caused by the tangential component of the gas velocity V_φ.

Figures 1-3 show the obtained distribution by the radius of the static pressure apparatus. Static pressure measurements were performed at six height levels (H = 0; 0,04; 0,08; 0,12; 0,16; 0,2 м).

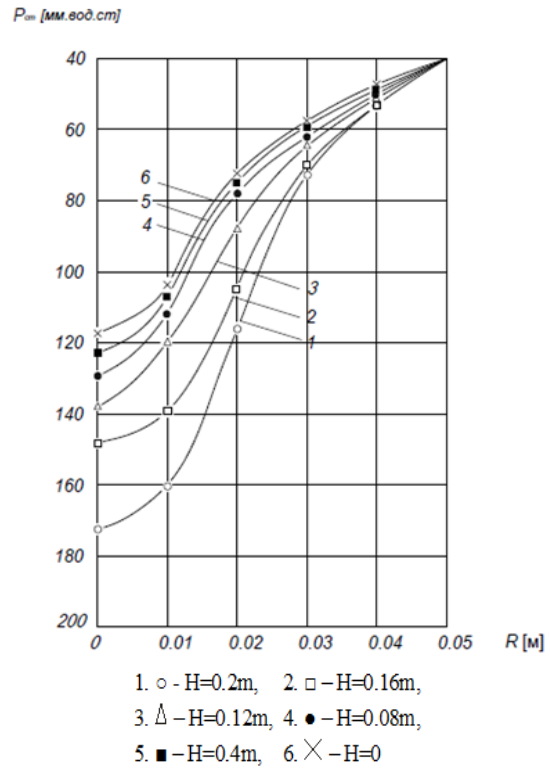

1. ○ - H=0.2m, 2. □ – H=0.16m,
3. △ – H=0.12m, 4. ● – H=0.08m,
5. ■ – H=0.4m, 6. ╳ – H=0

Fig. 1. Distribution of static pressure over the cross section of the apparatus VZP – 100 (K=0,61)

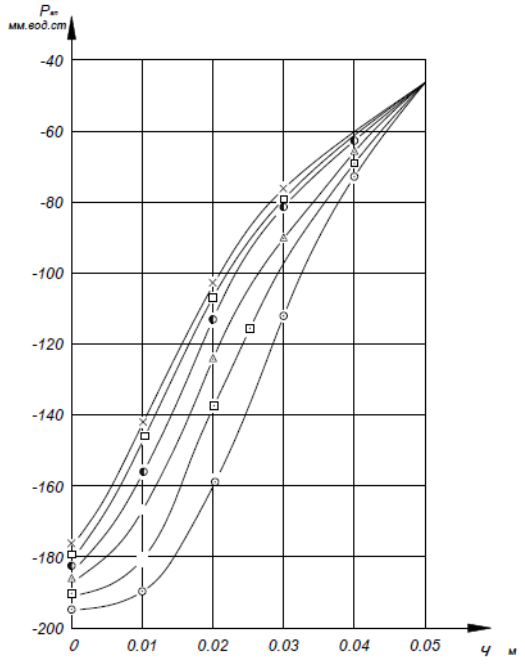

1. ⊙ - H=0.2, 2. □ – H=0.16,
3. △ – H=0.12, 4. ◐ – H=0.08,
5. ⊡ – H=0.4, 6. ╳ – H=0

Fig. 2. Distribution of static pressure over the cross section of the apparatus VZP – 100 (K=0,7)

As shown in the Figures, the static pressure profile depends on the ratio of costs through the channels of the apparatus ($\frac{Q_2}{Q}$ in experiments was 0,6; 0,7; 0,8). With increasing ratio of $\frac{Q_2}{Q}$ the pressure on the axis increases, and at the periphery (at the wall) decreases. With an increase of $\frac{Q_2}{Q}$ there is alignment of profiles P_{cm}.

First approximation of the distribution $P_{ст}$ can be described by solving the equation of radial equilibrium [9-15]

$$\frac{\partial P}{\partial r} = \rho_r \frac{V_\varphi{}^2}{r} \tag{5}$$

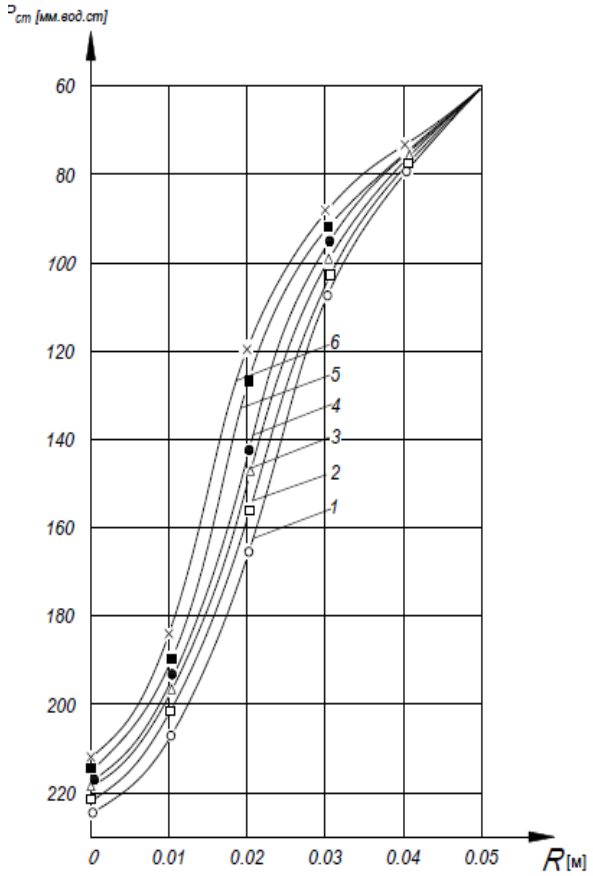

1. ○ - H=0.2m, 2. □ – H=0.16m,
3. △ – H=0.12m, 4. ● – H=0.08m,
5. ■ – H=0.4m, 6. × – H=0

Fig. 3. Distribution of static pressure over the cross section of the apparatus VZP – 100 (K=0,8)

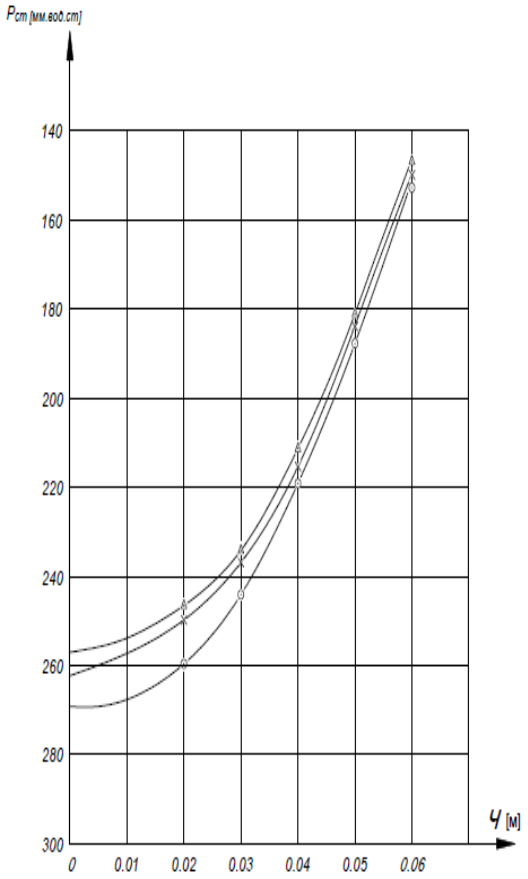

1. ⊙ - K=0.802
2. × – K=0.7
3. △ – K=0.6

Fig. 4. Static pressure distribution of the exhaust pipe section VZP – 200. Q = 0,22 m^3/c.

This equation satisfactorily describes the distribution of V_z up to, $r = r * y$ at the wall but the difference of 50%, which can be explained by the presence of turbulent pulsations, the action of which is largely affected by the walls of the apparatus [8, 9, 10].

Figure 4 shows that the static pressure distribution is obtained in the exhaust pipe of the VZP-200 dust collector, as seen from the representation distribution, with an increase in K the static pressure value at the axis of the pipe increases, at the periphery (at the wall of the pipe) the static pressure level is about the same (alignment of the profile occurs).

The graphs show that as the ratio of channel costs increases, the pressure loss (both in the separation volume itself and in the exhaust pipe) increases. This confirms once again the results obtained from the study of the pressure loss in the VZP.

Figure 5 shows the distribution of the axial velocity V_z by the cross-section radius at the input of the primary air flow. The maximum value of V_z is 0.035 m from the axis of the apparatus. As the K channel cost ratio increases, the axial speed of V_z is 0.035 m from the axis of the apparatus. As the K channel cost ratio increases, the axial speed of.

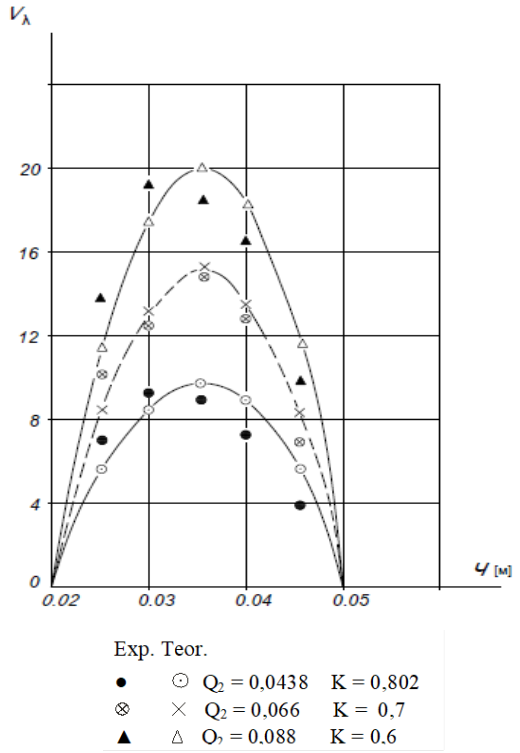

Fig. 5. Axial velocity distribution by cross-section radius at the exit from the primary input of the apparatus VZP – 200

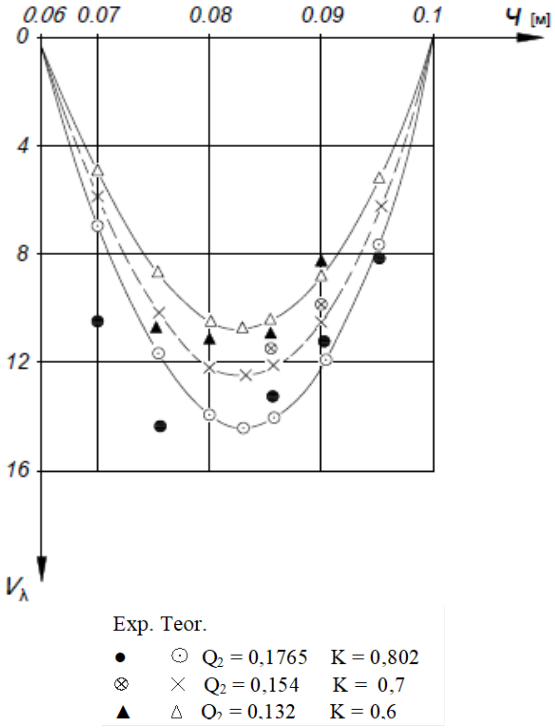

Fig. 6. Distribution of axial velocity by cross-section radius at the outlet from the secondary input of the apparatus VZP – 200

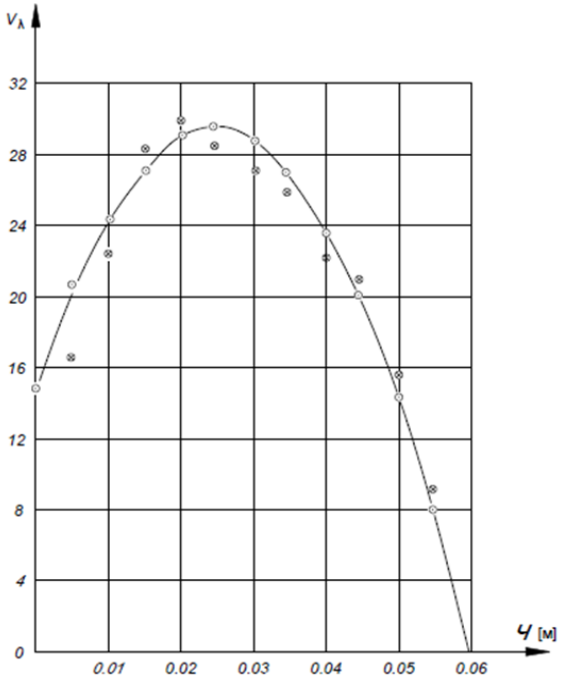

Fig. 7. Distribution of soy velocity by radius of exhaust pipe. Q = 22 m^3/c

Figure 6 shows the distribution of the axial component of the output velocity over the secondary input radius. The maximum value of V_z (minus) is 0.0825 m from the axis of the apparatus. With the increase of the share of secondary stream V_z (with minus) increases.
The results also correlate with capture efficiency and validate experimentally obtained data on capture efficiency in relation to the cost of the channels.
Figure 7 Shows the distribution of soy speed V_z and tangential speed $V\varphi$ on the radius of the exhaust pipe (the cross section is taken at a distance of 10 mm from the lower edge of the exhaust pipe).

4. Conclusion

Based on the data obtained, the following can be done:
1. The fields of static pressures in the apparatus of VZP have been determined and it has been established that with the increase of the ratio of streams, the difference of static pressure in the apparatus equalizes.
2. The distribution of static pressure over the cross section of the apparatus with different flow ratios is obtained.
3. A distribution of the axial velocity by the radius of the cross-section at the output from the primary and secondary inputs is obtained, and also by the radius of the exhaust pipe of the apparatus.
4. With the increase in the ratio of expenditures through the channels there is an increase in the loss of pressure, which confirms the results obtained in the study of the loss of pressure in the apparatus VZP.

References

1. M.-A. Etim, K. Babaremu, J. Lazarus, D. Omole, Health Risk and Environmental Assessment of Cement Production in Nigeria, *Atmosphere* **12**, 1111 (2021)
2. F. Perera, Pollution from Fossil-Fuel Combustion is the Leading Environmental Threat to Global Pediatric Health and Equity: Solutions Exist, *International Journal of Environmental Research and Public Health* **15**(1), 16 (2017)
3. X. Zhu, J. Yang, Q. Huang, T. Liu, A Review on Pollution Treatment in Cement Industrial Areas: From Prevention Techniques to Python-Based Monitoring and Controlling Models, *Processes* **10**, 2682 (2022)
4. A.G. Vetoshkin, Engineering protection of the atmosphere from harmful emissions, Infra-Engineering, Moscow (2016)
5. I.A. Popov et al., Study of velocity fields in devices with counter-twisted streams, Modern problems of textile industry development and tasks of engineering personnel training, MIT, Moscow (1979)
6. P.O. Ayegba, L.C. Edomwonyi-Out, Turbulence statistics and flow structure in fluid flow using particle image velocimetry technique: A review, *Engineering Reports* **2**, e12138 (2020)
7. I.L. Povkh, aerodynamic experiment in mechanical engineering, Mechanical engineering, Leningrad (1974)
8. N.A. Ivankov, D.S. Kiselev, Design and test results of the dust trap with regeneration of the bulk layer, *Machines and devices of chemical technology* **4**, 122-126 (1981)
9. R.B. Akhmedov et al., Aerodynamics of a twisted jet, Energy, Moscow (1977)
10. A. Sugak, E. Sugak, Centrifugal dust collectors and classifiers. Modeling, calculation, design, YAGTU, Yaroslavl (2012)
11. A.G. Vetoshkin, Dust cleaning processes and devices, Penza State Technical University, Penza (2005)
12. D.I. Misulya, V.V. Kuzmin, D.A. Markov, Comparative analysis of technical characteristics of cyclone dust collectors, *Chemistry and technology inorganic* **3**, 154-163 (2012)
13. O.S. Kochetov, M.O. Kochetov, T.D. Khodokova, Vorkhreva dust generator, Patent for invention RUS2256487, 15.06.2004.
14. B.S. Vas Black, L.I. Gudim, Dust catchers with counter-twisted streams, Tekhim Research Institute, Moscow (1982)
15. B.S. Sazhin, L.I. Gudim, Dust traps with counter-closed streams, *Chemical industry* **8**, 50-54 (1985)